4. Three-dimensional finite-element modeling of the glacial isostatic adjustment in Fennoscandia

Abstract[a]

During the last ice age cycles, large ice sheets have covered North America, Northern Eurasia, Greenland and Antarctica. The Earth's crust and mantle has been depressed by the weight of these ice sheets by several hundreds of meters. At the end of the last ice-age cycle, the ice sheets have vanished around 6000 years ago, and the Earth's surface rebounded. However, due to the time-dependent viscoelastic relaxation of the Earth's mantle, the rebound, also termed glacial isostatic adjustment (GIA), is still observable today. In Fennoscandia, a key region of GIA, numerous observations such as paleo-strandlines, present-day crustal deformations monitored by GPS observations, and present-day changes in the gravity field seen by satellite missions, provide a detailed picture of the past and ongoing deformation.

We model the GIA process in Fennoscandia by means of the finite-element technique. We employ a three-dimensional viscosity structure in the Earth's mantle derived from seismic shear-wave tomography models, and we use thermodynamic considerations to convert the shear-wave perturbations into viscosity variations. We then compare the results based on the three-dimensional Earth's structure with a simpler earth model, where viscosity depends on the vertical direction only. Our results indicate significant differences between three- and one-dimensional modeling:

The vertical crustal velocities reveal differences up to 7 mm/yr, and horizontal crustal velocities are effected even stronger. The typical divergent motions of the latter observed for one-dimensional earth models is no longer present for three-dimensional viscosity models. Instead, a regional velocity field with movements away from the Norwegian coast towards the old Baltic Shield is observed. In a sensitivity analysis we show that the dramatic change in the horizontal flow pattern has its origin deeper in the upper mantle, between 450 and 670 km depth. We also confirm that the observed GIA process in Fennoscandia is not very sensitive to the viscosity structure in the lower mantle. However, a comparison with BIFROST data reveals a best-fit with the simple, one-dimensional model, which requires a revision of our three-dimensional models in a future analysis.

[a] Steffen, Kaufmann and Wu (2006a). Three-dimensional finite-element modeling of the glacial isostatic adjustment in Fennoscandia, Earth Planet. Sci. Lett. **250**, 358-375.

4.1 Introduction

During the ice ages, large ice sheets covered North America, Northern Eurasia, Greenland and Antarctica repeatedly with a cyclicity of about 120,000 years. The solid Earth has been significantly deformed by the changing weight of these ice sheets on land and the water load in the oceans, as mantle material can flow on these timescales. While the last remnants of the Late Pleistocene ice sheets vanished around 6000 years ago, the Earth's surface is still readjusting from the last deglaciation event due to the time-dependent viscoelastic relaxation of the Earth's mantle. This process is called glacial isostatic adjustment (GIA).

Records of the crustal motion through observations such as paleo-shorelines (that indicate past sea-levels) and global positioning system (GPS) measurements (that map present-day crustal velocities) provide constraints to GIA modeling. In this paper, we focus on data in Fennoscandia since a large set of different observations, both in space and time, are available.

The observations of the GIA process constrain the material properties of the Earth, especially the mantle viscosity. As mantle viscosity can vary in all three dimensions, the observations are equally sensitive to radial and lateral changes of this parameter. However, the traditional theory of GIA has been developed for a one-dimensional (1D) earth model [Peltier, 1974; Farrell and Clark, 1976; Milne and Mitrovica, 1998], which greatly facilitates the computation. The improvement in computational power in the last decades allows the consideration of more complex two- (2D) and three-dimensional (3D) earth models, including lateral heterogeneities in lithospheric thickness and in mantle viscosity. Some representative examples for 2D and 3D GIA predictions will be discussed below:

The first investigations using 2D earth models were performed by Sabadini et al. [1986], Gasperini and Sabadini [1989], Sabadini and Gasperini [1989], Gasperini and Sabadini [1990] and Gasperini et al. [1991]. These authors used axi-symmetric finite-element (FE) models for a flat Earth and simple ice-load models to analyze the effects of lateral viscosity variations in the asthenosphere on model predictions. As a result, Sabadini et al. [1986] showed that a lithospheric thickness variation only weakly influences the deformation near the center of the former ice sheet. In contrast, the uplift near the edge of the ice load is extremely sensitive to lateral variations in lithospheric thickness and asthenospheric viscosity. Gasperini and Sabadini [1989] found a strong influence of lateral viscosity variations in the upper mantle on crustal deformations induced by the deglaciation. A comparison between radial and 2D viscosity models indicated that purely radial viscosity variations used in previous studies could possibly lead to a misinterpretation of GIA signals. Gasperini and Sabadini [1990] showed for lateral variations in viscosity that average viscosities in the upper and lower mantle depend on the magnitude and pattern of the heterogeneities in each layer. Gasperini et al. [1991] focused on effects of a high-viscosity craton below the lithosphere in Scandinavia. They concluded that close to the center of the former ice load, the stiffer region could be responsible for a reduction of one third in total vertical displacement and of an increase of one fourth in vertical velocity, which could affect the interpretation of relative sea-level (RSL) changes along continental margins and gravity anomalies in the center and along the peripheral regions.

Kaufmann et al. [1997] picked up the 2D modeling and used a 2D FE model with simple axisymmetrical ice-load histories and compared model predictions for both laterally homogeneous and heterogeneous earth models. They found that lateral heterogeneities in the lithosphere and asthenosphere, and also variations in lithospheric thickness, significantly influence the calculated land uplift and thus confirmed former results of Sabadini et al. [1986] and Gasperini and Sabadini [1989]. In addition, they showed that if the geological structure is known, a determination of lateral heterogeneities in lithospheric thickness

with a set of laterally homogeneous earth models is possible.

Wu et al. [1998] utilized for the first time 2D *and* 3D FE flat-Earth models, both with simple and realistic deglaciation histories to study the effects of lateral heterogeneities in earth rheology and density on geodetic signatures of the GIA process. The authors demonstrated with a 2D model that the effect of a low density continental root on geodetic data is generally small and that lateral variations in asthenospheric properties affect geodetic quantities more than lateral variations in lithospheric thickness. Using the 3D FE models, they confirmed these results. Furthermore, they found that lateral viscosity variations in the lower mantle have a larger effect on RSL data than heterogeneities only in the upper mantle. Thus, they advocated further studies especially for ice loads with size comparable to the Laurentide Ice Sheet.

Using a spherical spectral-FE 2D earth model, Martinec and Wolf [2005] showed that a model for Fennoscandia with a central 200 km thick lithosphere underneath the Gulf of Bothnia and a peripheral 80 km thick lithosphere underlain by a 100 km thick low-viscosity asthenosphere essentially gives the same response in the inverse relaxation time for the inverse relaxation-time spectrum (IRTS) as a 1D viscosity profile with a 100 km thick lithosphere and no asthenosphere.

More realistic, fully 3D ice and earth models for Fennoscandia were developed by Kaufmann et al. [2000] and Kaufmann and Wu [2002]. Kaufmann et al. [2000] also showed with these models that lateral variations in lithospheric thickness and asthenospheric viscosity do influence GIA predictions of paleo-shorelines and crustal motions. The difference in RSL predictions between radially symmetric models and models with a realistic 3D earth structure can be as large as 10 - 20 m. Also the predicted uplift rate and free-air gravity anomaly differ by 1 - 3 mm/yr and 2 - 4 mGal, respectively. For the first time, Kaufmann and Wu [2002] inverted synthetic RSL data, generated with a 3D earth model for the Fennoscandian region, for the best 1D radial viscosity profile and found that 1D earth models fail to correctly predict the correct values for lithospheric thickness and asthenospheric viscosities.

Several papers based on such flat 3D FE models considered other regions, e.g. the Barents Sea [Kaufmann and Wu, 1998a,b], Antarctica [Kaufmann et al., 2005] and Laurentia [Wu, 2005]. Kaufmann and Wu [1998a] investigated lateral viscosity variations across a continental margin and their influence on observable signatures of the GIA. They concluded that interpretations from laterally homogeneous models can be biased by effects arising from 3D viscosity structures in the Earth's mantle. Kaufmann and Wu [1998b] compared a laterally homogeneous and a laterally heterogeneous earth model and found a strong influence of lateral viscosity changes in the asthenosphere on uplift, present-day velocity and present-day gravity anomaly observations. Kaufmann et al. [2005] calculated the GIA induced crustal velocities and fault instability for a 1D and a 3D viscosity structure beneath Antarctica. The 3D earth model includes a stiff cratonic root underlying East Antarctica. As a result, the cratonic root induces a horizontal motion from East- to West Antarctica. The cratonic root also influences the fault stability offshore. Wu [2005] investigated the effect of lateral variations in lithosphere thickness and mantle viscosity on surface motions in Laurentia and found an influence on horizontal motion as well as on the uplift rate.

Wu [2002] extended the FE method to a 3D self-gravitating spherical earth model, which was coupled to the sea-level equation [Wu and van der Wal, 2003]. Completely introduced by Wu [2004], this method is called Coupled-Laplace Finite-Element Method. Wu and van der Wal [2003] and Wu et al. [2005] used this model approach and confirmed the results of flat 3D FE models. Their investigations found that effects of lateral viscosity variations in the deeper mantle are large.

Zhong et al. [2003] also developed a 3D spherical FE model with a 3D viscosity structure, but without the inclusion of the sea-level equation. In their paper, the authors investigated the role of laterally varying

lithosphere thickness. They showed that the effects of the lithospheric structure on the RSL change depend on the locations of the observation sites and on the size of loads.

Latychev et al. [2005b] developed a finite-volume (FV) formulation for 3D spherically symmetric, self-gravitating and elastically compressible earth model, which does not include self-gravity in the oceans. This model has been benchmarked by comparing a suite of predictions based on a spherically symmetric test model with results generated using the normal-mode approach [e.g. Mitrovica et al., 1994]. The first applications of their new FV method considered the effect of of lithospheric thickness variations [Latychev et al., 2005a] and of lateral viscosity variations in the mantle [Latychev et al., 2005b] on predictions of present-day 3D crustal velocities in North America. They found that lateral viscosity variations have a more significant impact on horizontal velocities than on radial velocities.

From the papers discussed above it is evident that a realistic 3D variation in mantle viscosity produces significantly different model predictions than a simpler 1D mantle-viscosity model.

One aim of this paper is to investigate how the thermodynamic properties of the mantle affect the background radial viscosity profile and also the inferred lateral viscosity variations. Another aim is to understand the relative importance between the contribution of the lateral viscosity variations in the various layers in the upper mantle and that from the lower mantle. Our focus will be on the GIA response induced by the melting of the Late Pleistocene Fennoscandian ice-sheet complex, based on realistic 3D viscosity distributions in the Earth's mantle. We employ a flat 3D FE model with compressible, viscoelastic material properties. It has been shown earlier that for GIA predictions in the Scandinavian region the flat-earth approach is adequate [e.g. Wolf, 1984; Amelung and Wolf, 1994; Wu and Johnston, 1998]. The GIA predictions of RSL change and crustal velocities are then compared to observed data of sea-level indicators and the BIFROST project. Our main emphasis is a comparison of a 1D and three 3D viscosity models. The 1D viscosity model is laterally homogeneous model, the 3D viscosity models are based on results of shear-wave tomography. For the 3D structure, different rheological reference models were used. In addition to the model comparison, we employ a sensitivity analysis for different mantle layers to localize regions, which influence the rebound pattern.

4.2 FE-model geometry

The GIA process in Fennoscandia is modeled using the FE method. A changing ice load is applied to the surface of a flat, viscoelastic earth model which has horizontal dimensions of 130,000 km and consists of 10 layers in the vertical direction, stretching from the Earth's surface to the core-mantle boundary at 2886 km depth. The generated mesh of $50 \times 50 \times 10$ hexahedra elements is divided into a central and a peripheral frame (Fig. 4.1). The 3000 km wide central frame, located in the center of the model, is meshed with 30 elements with a horizontal dimension of 100 km. The 10 elements of the 63,500 km wide peripheral frame have variable side lengths, increasing towards the edge. This huge horizontal dimension of the peripheral frame, which is about 10 times the Earth's radius is necessary, because viscoelastic investigations with flat FE models require an infinite horizontal extent, which can be modeled either using infinite boundary elements or, our choice, a surrounding frame with about 5 to 10 times the dimension of the area of interest. Both methods aim in allowing the mantle material to flow due to application of a surface load outside the area of interest. The first two vertical layers, with thickness values of 15 and 55 km, simulate the elastic lithosphere. The depth layers 3 to 6 with a total thickness of 600 km and the layers 7 to 10 with a total thickness of 2216 km represent the upper and lower mantle, respectively. The thickness values are summarized in Tab. 4.1. Rigid boundary conditions

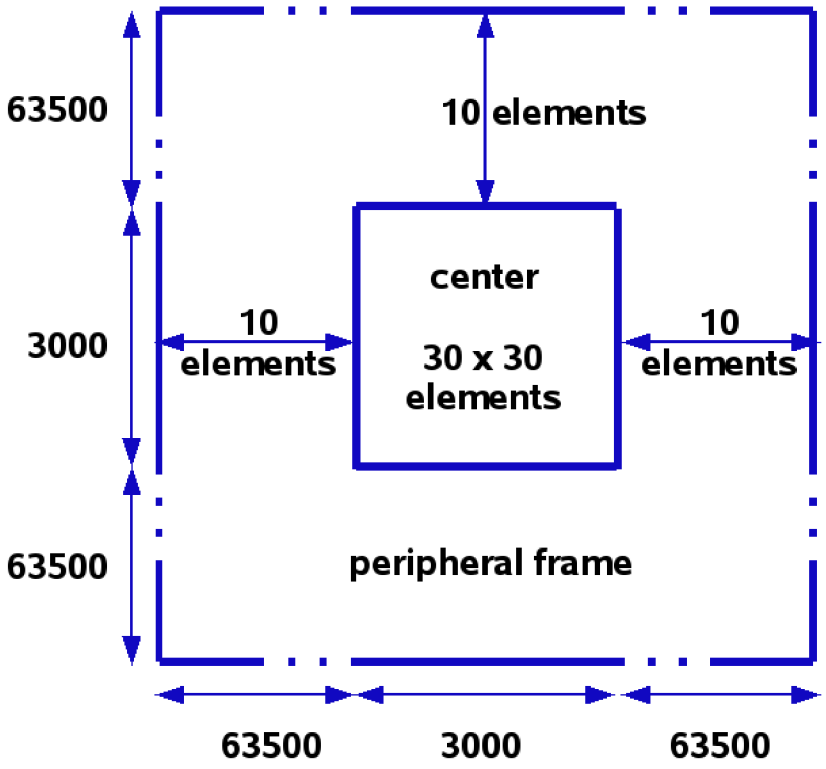

Figure 4.1: Sketch of the FE model geometry. Numbers on the left and bottom indicate the dimension in km.

are applied to the bottom and the sides of the model.

Table 4.1: Model dimensions and parameterization.

layer	thickness in m	depth in km	density in kg/m^3	Young's modulus in GPa	Poisson's ratio	
1	15	15	2653	75.3	0.278	lithosphere
2	55	70	3361	170.4	0.279	
3	176	246	3392	172.1	0.290	
4	204	450	3597	213.4	0.300	upper
5	100	550	3854	267.5	0.297	mantle
6	120	670	3974	305.5	0.295	
7	550	1220	4570	468.9	0.276	
8	580	1800	4880	559.6	0.288	lower
9	520	2320	5156	641.5	0.296	mantle
10	566	2886	5429	725.9	0.307	

4.3 Ice load

The ice model for the Late Pleistocene glacial history in Europe is taken from the FBKS8 ice model of Lambeck et al. [1998a], and applied within the central frame. The ice model FBKS8 simulates the extent and melting history of the Fennoscandian and Barents Sea Ice Sheets from the last glacial maximum (LGM) towards the present day. The extent of these ice sheets for four different epochs is shown in Fig. 4.2. The ice sheets are included in a high spatial and temporal resolution model that is consistent with the majority of the field evidence for ice-margin retreat and with the GIA data. The ice volume at the LGM approximately 22 000 years BP corresponds to 17 m of eustatic sea-level change. All reconstructions subsequent to the LGM are based on glaciological and geomorphological evidence and thus reflect the approximate extent of the Late Pleistocene ice sheets throughout the last glacial cycle. The time dependence of the load is applied as follows: A maximum load, corresponding to the LGM (at 22,000 years BP), is applied from 212,000 to 122,000 years BP. Then the load is instantly removed, and the model is ice free during the penultimate interglacial until 112,000 years BP. Then the load increases linearly, until it reaches its maximum extent at 22,000 years BP, followed by a detailed deglaciation history until the present. This parameterization has been shown to be sufficient to correctly predict changes in surface displacements [Kaufmann et al., 2000; Kaufmann and Wu, 2002]. In addition, we have tested our model adding a complementary ocean load. However, the effect of the ocean load on our present-day observables is one order of magnitude less than the ice-load signal and thus, the ocean load is not included in our load history.

4.4 Earth models

A layered, isotropic, compressible, Maxwell-viscoelastic half-space with a constant gravitational attraction of $g = 9.82$ m s^{-2} is used to model the glacially-induced perturbations of the solid Earth. We solve the Boussinesq problem for a layered, viscoelastic half-space using the commercial finite-element package ABAQUS [Hibbitt et al., 2005], which has been modified to include pre-stress in order to allow the deformed free surface to return to its initial equilibrium via viscous flow [Wu, 1992a,b, 2004]. Thus, the equation that describes the conservation of momentum is given by:

$$\nabla \cdot \sigma - g \nabla (\rho w) = 0, \tag{4.1}$$

where σ is the incremental stress tensor, ρ the density, g the gravitational acceleration, and w is the vertical displacement. The first term in equation (4.1), the divergence of stress, describes the surface force deforming the Earth. The second term arises because the undisturbed Earth is assumed to be in hydrostatic equilibrium, with the forces of self-gravitation balanced by the hydrostatic pre-stress. This pre-stress is being "advected" along with the material when the body deforms either elastically or viscoelastically. Thus, the second term in equation (4.1) represents the gradient of the "advected" pre-stress, $\rho g w$. The presence of this term is required in order to provide the buoyancy force that is needed to satisfy the boundary conditions in the fluid limit, and without this term, there would be no viscous gravitational relaxation. The validity of the finite-element model to predict glacial isostatic adjustment has been shown previously [Wu and Johnston, 1998].

Earth models consist of a layered elastic lithosphere over a layered viscoelastic mantle. Density ρ, shear modulus μ and bulk modulus κ are volume-averaged values derived from PREM [Dziewonski and Anderson, 1981] (see Tab. 4.1 for PREM density and elastic parameters). The density is considered to

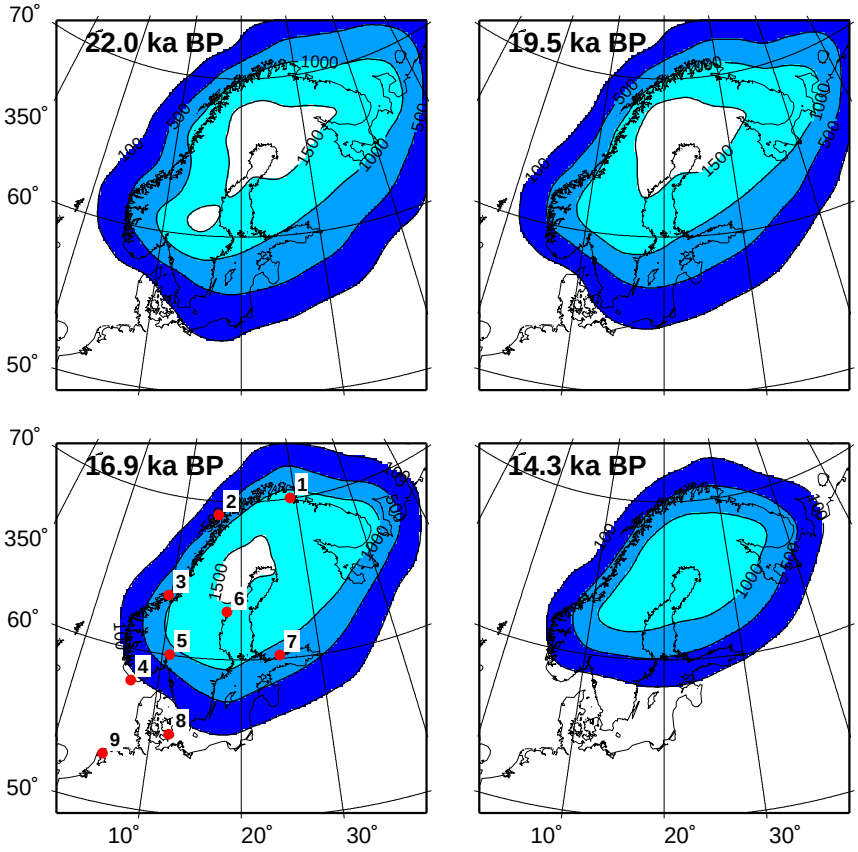

Figure 4.2: Map of ice model FBKS8 over Fennoscandia for four different time epochs. Contours are drawn every 500 m. Red dots mark selected locations with sea-level indicators.

be constant within an element. We compare two sets of earth models, 1D and 3D model sets, which will be discussed in the following sections.

4.4.1 1D viscosity profiles

Models U1L1_Vx, where U1 refers to a 1D upper mantle, L1 refers to a 1D lower mantle and Vx the vertical viscosity model number, represent laterally homogeneous reference models. The viscosity $\eta(z)$ varies in the vertical direction only. We define three different vertical viscosity profiles: The first profile, U1L1_V1, is characterized by only two different viscosity values, an upper-mantle viscosity of 4×10^{20} Pa s and a lower-mantle viscosity of 2×10^{22} Pa s (Fig. 4.3). This parameterization has been derived from fitting GIA observations of the Scandinavian region and has been confirmed by several independent studies [e.g. Lambeck et al., 1998a; Wieczerkowski et al., 1999; Milne et al., 2001; Kaufmann and Wu, 2002; Milne et al., 2004; Steffen and Kaufmann, 2005].

In the second profile, U1L1_V2, the radial viscosity has been derived from an Arrhenius-law:

$$\eta(z) = \eta_0 \exp\left(\frac{E(z) + p(z)V(z)}{RT(z)}\right), \tag{4.2}$$

Here, z is depth, η_0 is a scaling parameter, E the activation energy, p the pressure, V the activation

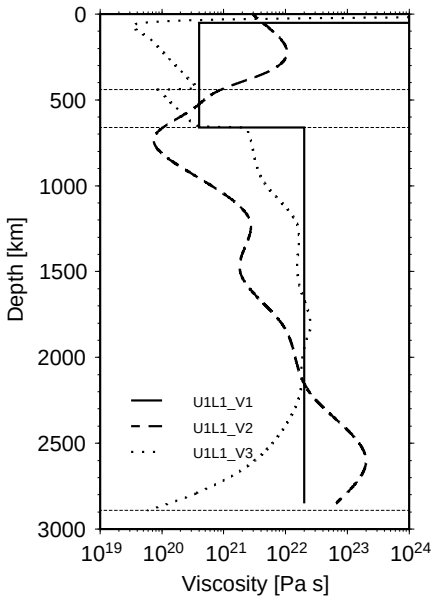

Figure 4.3: Radial viscosity profiles $\eta(z)$ as a function of depth.

volume, R the gas constant, and T the temperature. The parameters used are an activation enthalpy $E + pV$ tabulated in Ivins and Sammis [1995](Fig. 4.4b), and a temperature profile derived from a mantle convection model described in Leitch and Yuen [1989] (Fig. 4.4d). The second viscosity profile is characterized by a relatively high viscosity in the uppermost mantle, a pronounced low-viscosity region ($\simeq 10^{20}$ Pa s) below the 660 km discontinuity, and a high viscosity above 10^{22} Pa s in the lowermost mantle (Fig. 4.3).

The third profile, U1L1_V3, is based on the activation energy and volume for olivine from Karato and Wu [1993] for the upper mantle, and the activation enthalpy for perovskite from Yamazaki and Karato [2001] for the lower mantle (Fig. 4.4b). The temperature profile has been derived by solving the heat conduction problem in the lithosphere and the D"-layer, and an adiabatic gradient in the mantle, including the two phase transitions (Fig. 4.4d). It is characterized by a low viscosity ($< 10^{19}$ Pa s) directly beneath the lithosphere, then generally increasing towards mid-mantle depth to values above 10^{22} Pa s in 200 km depth (Fig. 4.3). At the two phase transitions, viscosity jumps by half an order of magnitude.

In both U1L1_V2 and U1L1_V3 the viscosity scaling parameter η_0 is chosen to satisfy the Haskell constraint of $\overline{\eta}(z) = 10^{21}$ Pa s [Mitrovica, 1996], which is a classic and enduring inference of mantle viscosity. Therefore, the viscosity profile between 100 km and 1400 km depth is shifted, until the volume-averaged viscosity in that depth range is equal that value.

4.4.2 3D viscosity structures

We then define the 3D viscosity model as the product of viscosity variation $\Delta\eta(x,y,z)$ and the vertically-dependent viscosity profile $\eta(z)$:

$$\eta(x,y,z) = \eta(z) \times \Delta\eta(x,y,z), \tag{4.3}$$

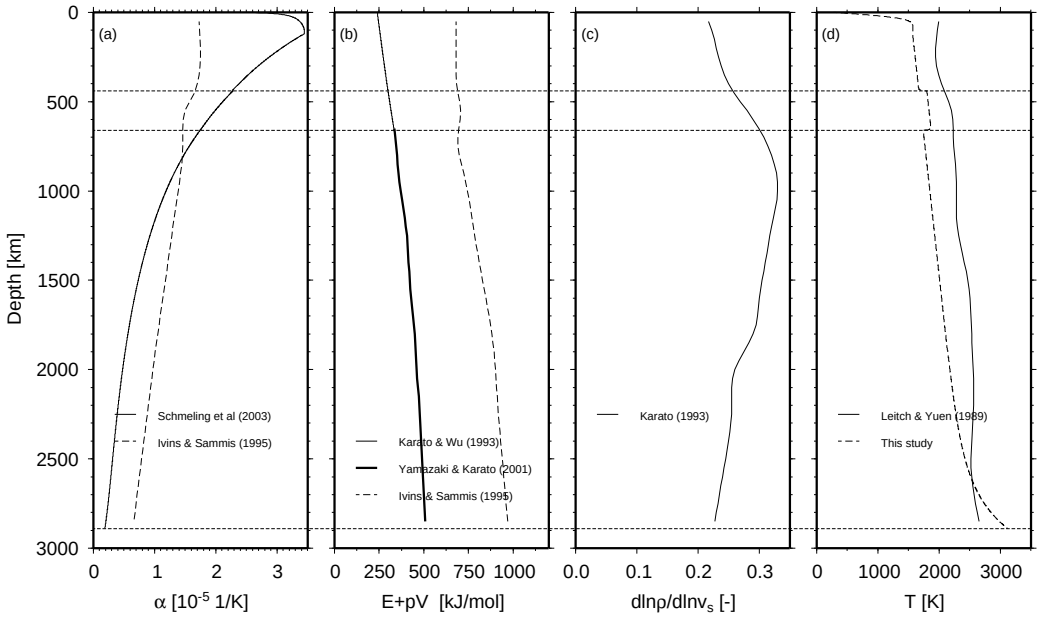

Figure 4.4: (a) Thermal expansivity α as a function of depth. (b) Activation enthalpy $E + pV$ as a function of depth. (c) Density-to-shear-wave velocity conversion $d\ln\rho/d\ln v_s$ as a function of depth. (d) Temperature T as a function of depth.

with x and y the horizontal dimensions. The 3D viscosity variation $\Delta\eta(x,y,z)$ is derived from the shear-wave velocity perturbations in the S20A tomographical model [Ekström and Dziewonski, 1998] by the following scaling relationship [for details see Ivins and Sammis, 1995; Kaufmann et al., 2005]:

$$\Delta\eta(x,y,z) = \exp\left(\frac{E(z)+p(z)V(z)}{R}\frac{1}{\alpha(z)}\frac{1}{T(z)^2}\frac{d\ln\rho}{d\ln v_s}(z)d\ln v_s(x,y,z)\right), \tag{4.4}$$

with α the thermal expansivity (see Fig. 4.4a), and $d\ln v_s$ the shear-wave velocity perturbations from S20A. The density-to-velocity conversion, $\frac{d\ln\rho}{d\ln v_s}$, is taken from Karato [1993] (Fig. 4.4c). This equation assumes that the lateral variations in seismic velocities seen in seismic tomography are caused by lateral temperature variation only.

Five different 3D viscosity structures are used in this paper (see Tab. 4.2):

U3L3_V1 is based on the vertical viscosity profile U1L1_V1 with its fixed values for the upper and lower mantle. The thermal parameters needed for the 3D variations (eq. 4.4) are a thermal expansivity and an activation enthalpy tabulated in Ivins and Sammis [1995] (Fig. 4.4a and b), and the temperature profile from Leitch and Yuen [1989]. The resulting viscosity structure, binned into four depth intervals in the upper and lower mantle, respectively, is shown in Fig. 4.5. The most striking feature is the high-viscosity region in the 70 - 250 km depth interval underneath the eastern part of Scandinavia. This high-viscosity region correlates with the cold, stiff Baltic Shield, and results from the strong shear-wave perturbations in the tomographical model. Towards the Mid-Atlantic ridge, viscosities in that depth decrease by several orders of magnitude. In the remaining upper mantle bins, lateral viscosity variations are moderate, mostly confined to a variation of one order of magnitude around the 1D profile. These small lateral variations continue into the lower mantle, only in the lowermost mantle (2300 - 2850 km depth bin) they become larger.

Table 4.2: Used viscosity models for calculation and references for input parameters. Abbreviations: IS = Ivins and Sammis [1995], LY = Leitch and Yuen [1989], KW = Karato and Wu [1993], YK = Yamazaki and Karato [2001], SKW = this study, K = Karato [1993], Sch = Schmeling et al. [2003]

.

		E + pV	T	α	$\frac{d\ln\rho}{d\ln v_s}$
1D	U1L1_V1	-	-		
	U1L1_V2	IS	LY		
	U1L1_V3	KW+YK	SKW		
3D	U3L3_V1	IS	LY	IS	K
	U3L3_V2	IS	LY	IS	K
	U3L3_V3	KW+YK	SKW	Sch	K

In U3L3_V2, the thermal dependencies for the lateral viscosity variation (eq. 4.4) are the same as above, only the 1D viscosity profile U1L1_V2 is different. Hence, the pattern of the 3D viscosity structure is very similar, with the high-viscosity region underneath the lithosphere, and smaller variations through the remaining mantle (Fig. 4.6). However, the absolute viscosity values differ: For example, between 250 - 450 km depth, model U3L3_V2 is about one order of magnitude more viscous than model U3L3_V1, between 550 - 1200 km depth it is one order of magnitude less viscous (see Figs. 4.5 and 4.6).

U3L3_V3, however, is strikingly different (Fig. 4.7). This model is based on the 1D viscosity profile U1L1_V3, while the thermal parameters for the 3D variation are a thermal expansivity taken from Schmeling et al. [2003], which is pressure- and temperature dependent. The temperature-dependence has a pronounced effect, as it can be seen in Fig. 4.4a: In the uppermost mantle, α increases by a factor of two, when compared to the previously used profile. The activation enthalpy is based on the perovskite model of Yamazaki and Karato [2001]. It is around fifty percent smaller than the estimate from Ivins and Sammis [1995] (Fig. 4.4b). The temperature profile is based on the mantle adiabat (Fig. 4.4d), which,

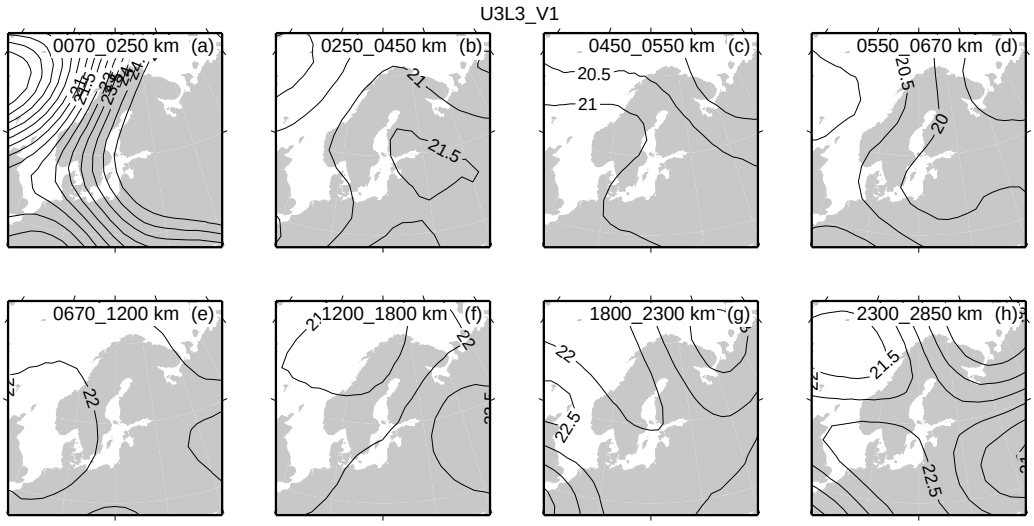

Figure 4.5: Viscosity structure U3L3_V1 for eight depth intervals. Contours show the logarithm of viscosity $log_{10}\eta$.

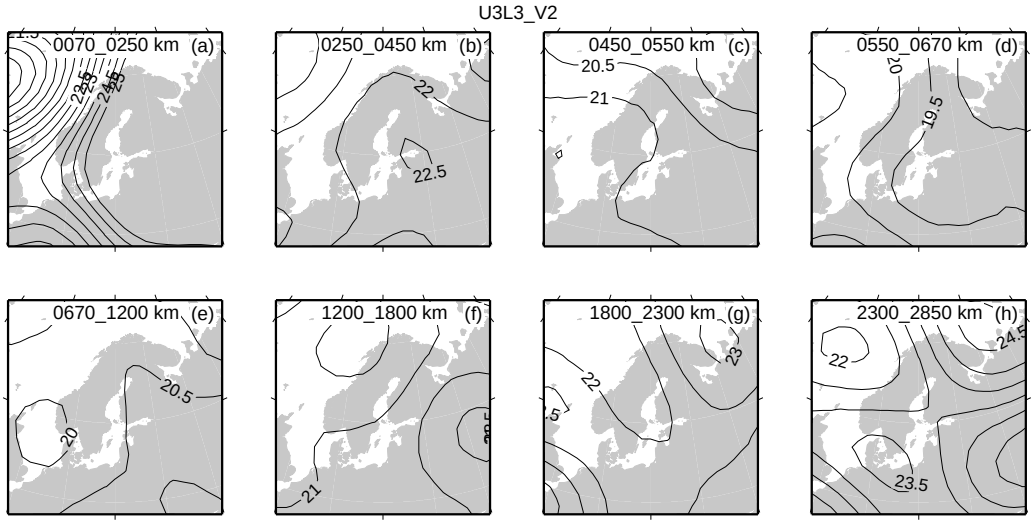

Figure 4.6: Same as Fig.4.5, but for model U3L3_V2.

however, is similar to the temperature inferred from the mantle convection model. As a result, the higher thermal expansivity together with the lower activation enthalpy reduce the effect of lateral viscosity variations in the uppermost mantle, as it can be seen in Fig. 4.7. The cratonic root in the first depth bin is much less pronounced now, and in the remaining upper mantle lateral viscosity variations are less than one order of magnitude. In the lowermost mantle below 1200 km depth, the lateral viscosity variations become larger and are similar to the variations of the two other structures.

The remaining two viscosity structures used are modifications of model U3L3_V1: In U3L1_V1, lateral viscosity variations are only taken into account in the upper mantle, while in U1L3_V1, only the lower mantle has a 3D viscosity structure.

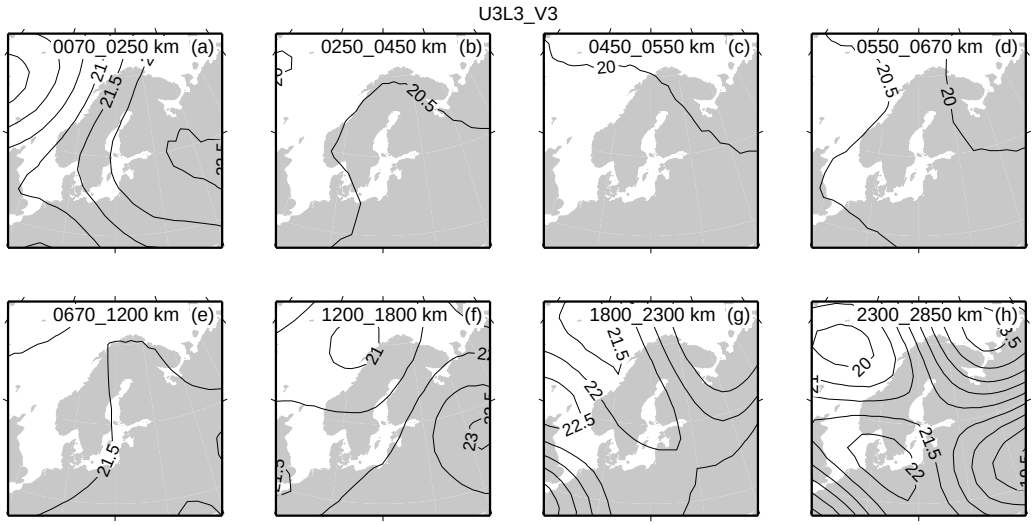

Figure 4.7: Same as Fig.4.5, but for model U3L3_V3.

In section 4.5.3, we also consider lateral heterogeneous models U3*n*L1_V1, which are similar to model U3L1_V1, except that the lateral viscosity variations are restricted to layer n =1, 2, 3 or 4 in the upper mantle, respectively.

4.5 Results

In this section we discuss the modeling results of six different earth models, the five models with 3D viscosity structure mentioned above and the 1D model U1L1_V1 as a simple case for a comparison between 1D and 3D viscosity structures. The 1D models U1L1_V2 and U1L1_V3 are not used for calculation as they only provide the base for the development of the 3D models U3L3_V2 and U3L3_V3, respectively. The model predictions of present-day motions (uplift and horizontal movement) for the Scandinavian region are compared with results of the BIFROST project [Johansson et al., 2002] as well as predicted sea-levels with observed data of sea-level indicators.

4.5.1 1D earth model

We start with the results arising from 1D model U1L1_V1.

Present-day motion. In Fig. 4.8 the predictions of the remaining uplift (left) as well as of the horizontal and vertical movement (right) are illustrated. The contours indicate the vertical uplift rate and the arrows the horizontal velocities. They show a positive uplift rate in the center of the former ice sheet of more than 10 mm/yr with a residual of more than 80 m, which corresponds to a ∼11 mGal gravity anomaly. The zero contour of the vertical movement can be traced around 400 km away from the Norwegian coast, through Denmark and Northeastern Germany, Poland, Belarus and Russia. Small subsidence with magnitude much less than 2 mm/yr characterizes the regions beyond. Small horizontal movements are

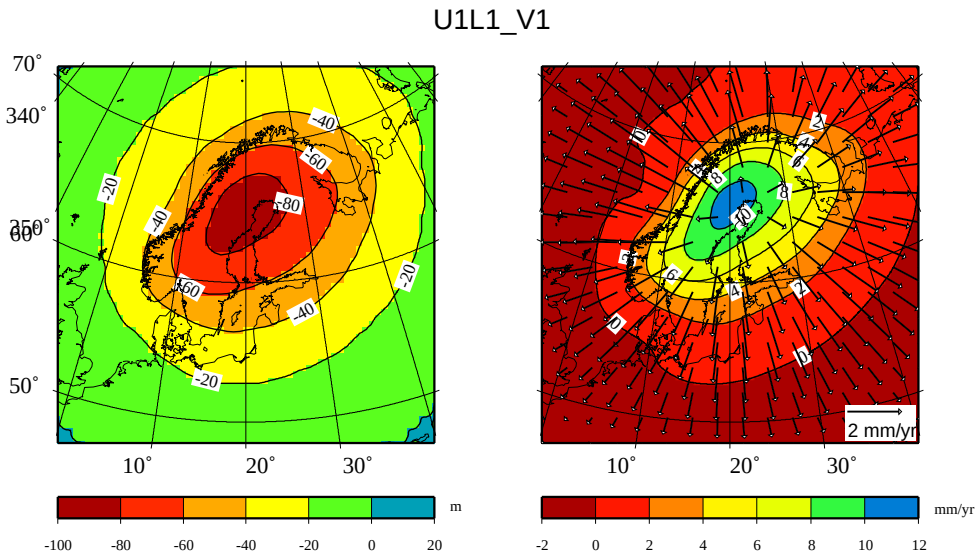

Figure 4.8: Predictions of residual uplift (left, contours) and of horizontal and vertical movement (right, contours and arrows) for the 1D model U1L1_V1.

established in the center and the outer regions of the modeled area. The largest horizontal movements result around 5 mm/yr at the Norwegian coast. The present-day motion indicates a divergent signature from the center of the former ice sheet (NW Golf of Bothnia) towards the outer regions.

Fig. 4.9 shows the observed vertical and horizontal motion in Fennoscandia obtained from the BIFROST campaign [Johansson et al., 2002]. The observations are compared to the predicted motion for the 1D viscosity model U1L1_V1. The center of the predicted uplift lies northwest of the observed uplift center, which is due to the ice sheet model. This is the reason for a difference in the uplift rate of around 2 mm/yr for most of the BIFROST locations situated near the center. Besides this, the maximum uplift rate of more than 10 mm/yr can be reproduced with the 1D model. The horizontal movement shows a divergence from the center, but amplitudes of northwestern BIFROST stations are larger than the calculated. Furthermore, the model indicates large movements by nearly 2 mm/yr to southeast in Southern Sweden and Denmark, which is not observed with BIFROST data.

Sea-level change. In Fig. 4.10, predicted relative land uplift curves for the models based on the viscosity structure V1 are compared to the relative sea-level data (black dots) at nine selected locations of Fennoscandia and northwestern Europe (see Fig. 4.2). The sea-level observations are corrected for a spatially uniform eustatic sea-level change [see Kaufmann and Wolf, 1996, for correction details], and are taken from a database compiled by Tushingham and Peltier [1992], chosen to cover the formerly ice sheet area fairly evenly. They have been converted from the radiocarbon timescale to the U/Th timescale, using the CALIB-4 program [Stuiver and Reimer, 1993; Stuiver et al., 1998]. We are using these data only to indicate the deviation between model predictions, because matching of the observations within their uncertainties by model predictions is achieved much better with a spherical earth model and a realistic load model for the Late Pleistocene ice-ocean mass balance.

The trend of monotonic land uplift indicated at the locations Helsinki, Oslo Fjord, Ångermanland, Varanger Fjord, And Fjord and Bjugn as well as the land subsidence at the locations of Praesto and

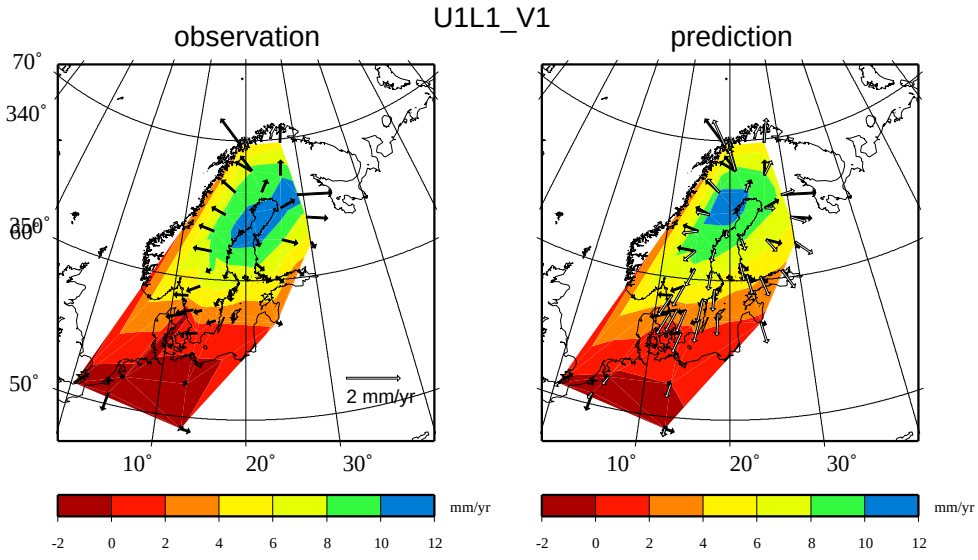

Figure 4.9: BIFROST uplift and horizontal motion data (left) and model prediction from the 1D model U1L1_V1 (right). Contours indicate the vertical motion, the black arrows the horizontal motion derived from BIFROST and white arrows the predicted horizontal motion in mm/yr.

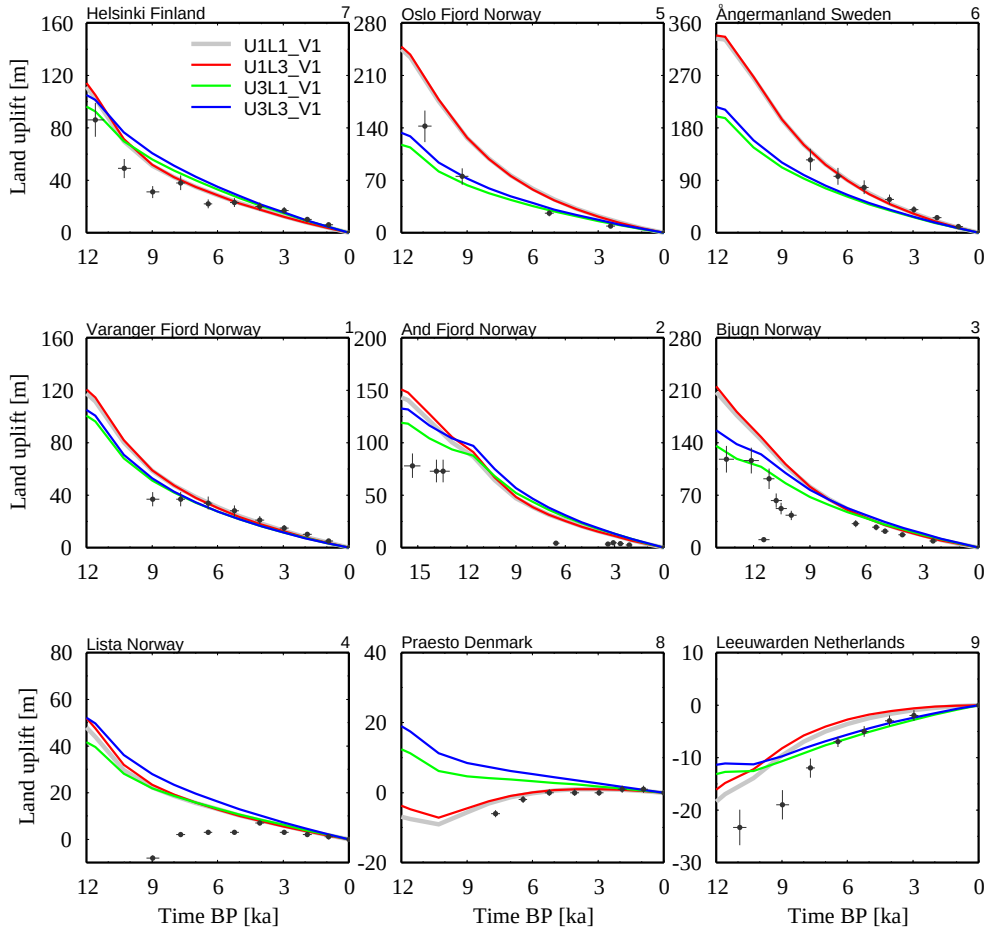

Figure 4.10: RSL observations (black dots with error bars) at selected locations on Fennoscandia compared to the predicted sea-level results from the models U3L3_V1 (blue lines), U3L1_V1 (green lines), U1L3_V1 (red lines) and U1L1_V1 (grey lines). Numbers indicate the locations in Fig. 4.2.

Leeuwarden agree well with the model predictions of U1L1_V1 (grey line). Greater differences can be found at Lista, where uplift instead of subsidence is predicted. The discrepancies between observations and predictions are possibly a consequence of the coarseness of the FE grid of the ice model, and in minor parts due to the not perfectly corrected eustatic sea-level change in the sea-level data. Nevertheless, the good fit in the trend of prediction and observation is also due to the ice model, which was constructed with the help of a 1D earth model to fit the sea level [see Lambeck et al., 1998a, for more information]. This earth model with a lithosphere thickness H_l of 75±10 km, an upper-mantle viscosity η_{um} of 3.6×10^{20} Pa s and a lower-mantle viscosity η_{lm} of 0.8×10^{22} Pa s is comparable to the used one in this work ($H_l = 70$ km, $\eta_{um} = 4 \times 10^{20}$ Pa s, $\eta_{lm} = 2 \times 10^{22}$ Pa s). Hence, our model is able to compute a consistent sea level for a flat earth model.

4.5.2 3D earth models

In this section, we investigate the effects of lateral variations in mantle viscosity on predictions of present-day velocities and RSL change.

Present-day motion. In Fig. 4.11 the predictions of the horizontal (arrows) and vertical velocities (contours) at the BIFROST locations for the six models are plotted. A comparison of the results for the models U1L1_V1 (top left) and U1L3_V1 (middle left) shows a good agreement in land uplift. The agreement at the highest peak is around 98% and is due to the low resolving power of surface motion to the lower-mantle viscosity structure. In contrast, the models U3L3_V1 (top right) and U3L1_V1 (bottom left), which include lateral viscosity variations in the upper mantle, show smaller values for the uplift rate. For both models, at most around 8 mm/yr are predicted, a difference of 2 mm/yr when compared to models U1L1_V1 and U1L3_V1. The horizontal motions are strikingly different for models U1L1_V1 and U3L3_V1 (and also for U3L1_V1). Both predict the divergent movement from the center, but in the northwest of the Scandinavian peninsula a north-directed motion with values at most around 1.2 mm/yr for a 3D upper mantle can be found, in contrast to the west and northwest movements of around 1.2 mm/yr determined with models U1L1_V1 and U1L3_V1. Including a 3D upper mantle, the southern locations of Sweden are characterized by a smaller (around 0.8 mm/yr), more southward directed horizontal motion. The predicted horizontal motions at locations in central Europe are directed towards northwest with at most 0.4 mm/yr. In contrast, for models with a homogeneous upper-mantle viscosity structure a completely different movement is found, which is directed to the southwest with values around 1.6 mm/yr.

The results obtained with background viscosity structures following method V2 and V3 strongly differ from the V1 results. For model U3L3_V2 (middle right), the uplift predicted is at most around 3 mm/yr, less than a third of the observed maximum. The reduced uplift results from the stiffer upper mantle, which is at least one order of magnitude greater than for the V1 model. For horizontal motions velocities mostly around 0.2 mm/yr are predicted, indicating a movement to the northeast in contrast to the divergence obtained with V1 models. In general, model U3L3_V2 cannot explain recent observed movements of Fennoscandia.

For model U3L3_V3 (bottom right), predictions of more than 8 mm/yr for the uplift rate results, but the center of the uplift is situated in the center of the Scandinavian Peninsula, which is 200 km west from the observed uplift center in the Golf of Bothnia. The predicted horizontal movements have a maximum value of 0.7 mm/yr, which are higher than the ones predicted for model U3L3_V2, but still smaller (by around two third) than for the models with viscosity structures following method V1. The horizontal movement indicates a divergence near the uplift center as for model U3L3_V1, but southeastern locations show small values directed towards southwest, induced by the given viscosity structure in the upper two layers. Compared with the observations, the predicted horizontal velocities as well as the vertical uplift rate are too small.

Sea-level change. In Figs. 4.10 and 4.12, a comparison between predicted sea-levels at nine selected locations in Fennoscandia and Central Europe is made. The comparison in Fig. 4.10 indicates on the one hand a similar behavior for viscosity models with a lateral upper-mantle viscosity variation (U3L3_V1, blue lines; U3L1_V1, green) and on the other hand with a fixed 1D upper-mantle viscosity (U1L1_V1, grey; U1L3_V1, red). The predictions for models U1L1_V1 and U1L3_V1 differ at most around 8 m at And Fjord about 16,000 years BP. Larger differencesbetween the two models with heterogeneous upper mantle can mostly be found before 6000 years BP, with a maximum difference of 20 m at Bjugn. Obviously, the two models with heterogeneous upper-mantle viscosities are characterized by greater differences in their predictions than the two models with homogeneous upper-mantle structures, confirming no strong influence of sea-level data by (1) a lateral lower-mantle viscosity variation and (2) the lower mantle itself. Large differences between results of models with homogeneous and heterogeneous upper mantle are also clearly seen, e. g. more than 120 m at Oslo Fjord and Ångermanland. At Bjugn, the dif-

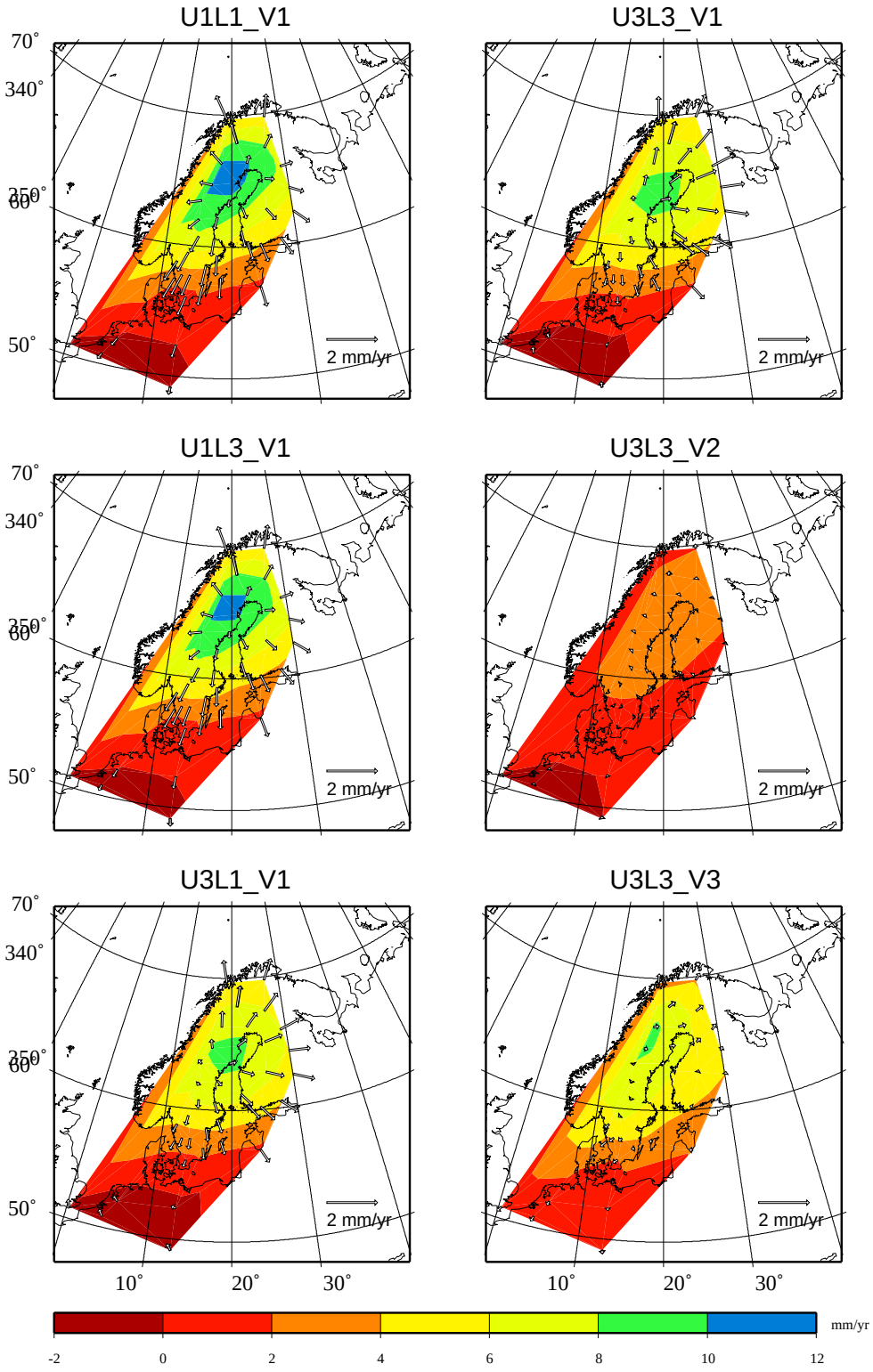

Figure 4.11: Predictions of horizontal and vertical velocities for different earth models. Contours indicate vertical and arrows horizontal velocities (in mm/yr).

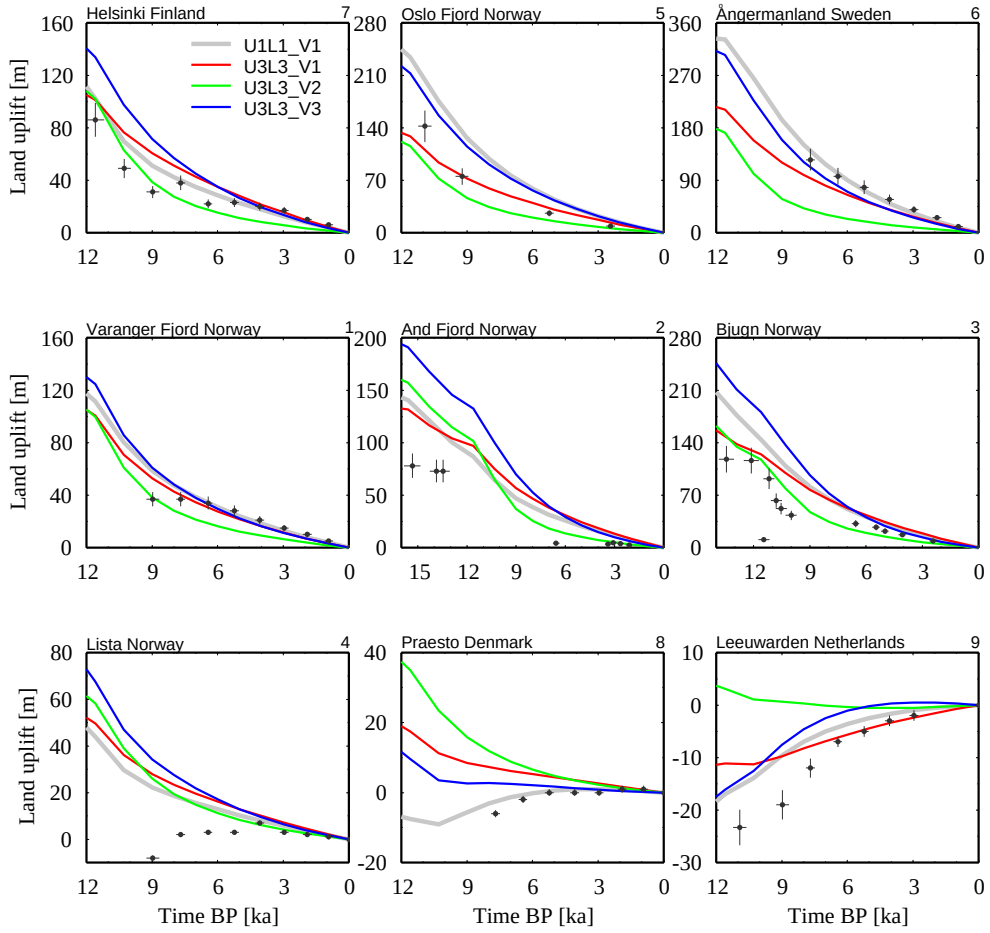

Figure 4.12: RSL observations (black dots with error bars) at selected locations on Fennoscandia compared to the predicted sea-level results from the models U3L3_V1 (red lines), U3L3_V2 (green lines), U3L3_V3 (blue lines) and U1L1_V1 (grey lines). Numbers indicate the locations in Fig. 4.2.

ference is about 80 m, at Helsinki, Varanger Fjord, And Fjord and Praesto, the differences are between 20 m and 30 m. At the locations of Lista and Leeuwarden, the differences are between 8 m and 10 m. Near the position of the former ice sheet, the models with homogeneous upper-mantle viscosity structure show larger land uplift values due to the weaker 1D viscosity. The average 3D viscosity is higher than the 1D (see Fig. 4.5) and therefore, the land uplift is much smaller. Furthermore, at the location Lista none of the models correctly predicts the sea-level observations. As explained earlier, this is due to the limitation of the FE grid in simulating the coast line. In summary, the results of the models U1L1_V1 and U1L3_V1 with a homogeneous upper mantle better fit with the sea-level observations, which is due to the fact that ice model FBKS8 was constructed based on the background earth model and the same RSL data (see section 4.5.1, sea-level change).

In Fig. 4.12 the predicted sea-level curves for the 1D model U1L1_V1 (grey) and the 3D models U3L3_V1 (red), U3L3_V2 (green) and U3L3_V3 (blue) are compared. The predictions of model U3L3_V2 with high background viscosities in the upper mantle differ significantly from the predictions of other models for most of the sites. Compared to the 1D model, differences up to more than 150 m at Ångermanland are found. Comparing U1L1_V1 to the 3D model U3L3_V3 remarkable values

of around 130 m are found there. The predictions of model U3L3_V2 are generally closer to that for 3D model U3L3_V1. The stiffer upper mantle of method V2 allows only a small deformation by the former ice sheets, resulting in values less than 200 m for land uplift in Ångermanland 15,000 years BP. For locations beyond the former ice sheet (Lista, Praesto, Leeuwarden) the trend is not traced.

Sea-level predictions of model U3L3_V3 mostly follow the predictions of the 1D model. At Oslo Fjord, Helsinki, Varanger Fjord, Ångermanland and Lista, the differences range between 20 m to 30 m. More than 40 m are determined at Bjugn and And Fjord, less than 20 m at Praesto. A good agreement between the predictions of the models U1L1_V1 and U3L3_V3 is established at Leeuwarden with at most 3 m. The good fit with the predictions of the 1D model is caused by only small variations in upper-mantle viscosity for method V3 and the much less pronounced cratonic root in the first depth bin, which is more in line with a homogeneous upper mantle structure.

4.5.3 Sensitivity of GIA predictions to upper-mantle viscosity structure

From the previous subsection, it is clear that GIA observations in Fennoscandia are not sensitive enough to resolve the viscosity structure of the lower mantle. On the other hand, the effect of lateral viscosity variations in the upper mantle on relative sea levels and present-day velocities is strong, which confirms earlier results of Gasperini and Sabadini [1989], Kaufmann et al. [1997], Kaufmann and Wu [1998b], Kaufmann et al. [2005], and Wu [2005]. Thus, in this subsection we use the subdivision of the upper mantle into the four depth bins depicted in Fig. 4.5 to investigate the sensitivity of GIA predictions depending on the lateral viscosity structure in these individual depth bins.

In Fig. 4.13, model predictions of the vertical (contours) and horizontal (arrows) velocity are shown. The top row depicts our already discussed 1D viscosity model U1L1_V1 (top left) and the 3D viscosity model U3L1_V1 (top right). The model response of the latter one has been shown to be very similar to U3L3_V1. In the middle and bottom rows, models, in which only one of the four upper-mantle depth bins has a 3D viscosity structure, are termed U3nL1_V1, with $n = 1,4$ the depth-bin counter.

In model U31L1_V1 (middle left), the bin between 70 and 250 km depth has a 3D viscosity structure. For this model, the uplift velocities are reduced to a maximum of 8 mm/yr, when compared to the 10 mm/yr for the 1D model U1L1_V1. The reduction is related to the stiffer uppermost mantle. The general pattern of horizontal velocity predictions for U31L1_V1 is similar to the patterns for the 1D model. However, deviations can be found along the Norwegian coast in the west, where the 3D model results in lower horizontal velocities. In general, however, the very high viscosity of model U31L1_V1 in the region of the Baltic Shield with viscosities up to 10^{25} Pa s produces a very thick ($>$ 200 km), almost elastic lithosphere in the eastern parts of Fennoscandia, acting as a plate.

For model U32L1_V1 (middle right), the depth bin between 250 and 450 km has a 3D viscosity structure. Here, the vertical velocities of up to 12 mm/yr are higher, when compared to the 1D model U1L1_V1. Horizontal velocities in the East and Southeast of Fennoscandia are reduced as a result of the high viscosity in the second bin of the 3D model U32L1_V1.

The vertical velocity predictions for 3D model U33L1_V1 (bottom left) are almost similar to the ones for 1D model U1L1_V1. However, when we compare the horizontal velocities of this 3D model to the 1D model, we observe a slight reduction over Central Sweden, where viscosities in the 3D model are higher, and an increase in horizontal velocities over Northeast Finland, where viscosities are lower, when compared to the 1D model.

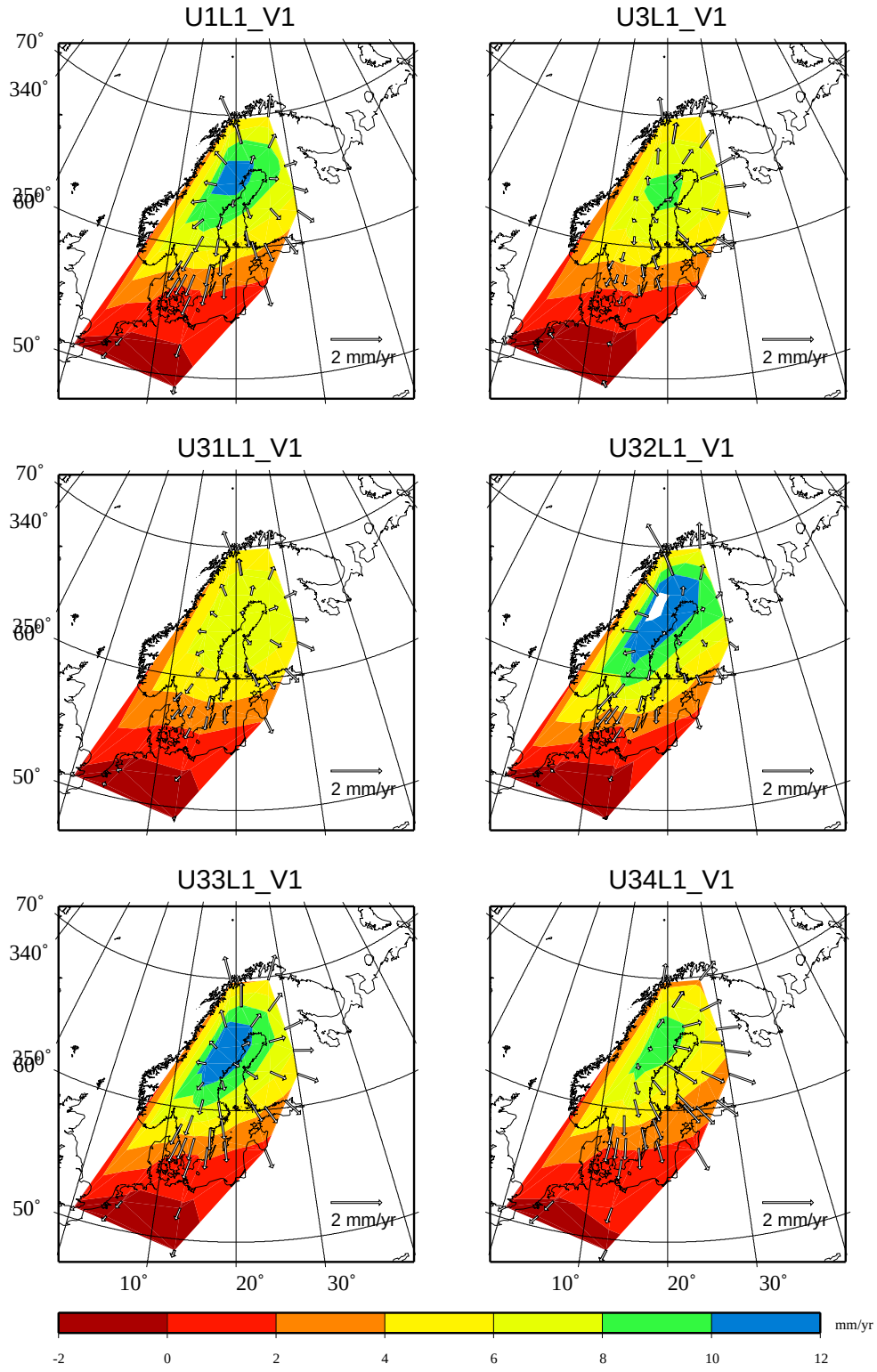

Figure 4.13: Predictions of horizontal and vertical velocities for Earth models with only one 3D layer and models U1L1_V1 and U3L1_V1. Contours indicate vertical and arrows horizontal velocities (in mm/yr).

Finally, a pronounced effect in both vertical and horizontal velocities can be observed for 3D model U34L1_V1 (bottom right). The vertical velocities are reduced by 2 mm/yr due to the weaker viscosity underneath Central Fennoscandia in the bin between 550 and 670 km depth. Even more impressive, the horizontal velocities show a strong asymmetry, with negligible velocities along the Caledonian Mountains between Norway and Sweden, but large eastward-directed velocities for the Baltic Sea and Finland. This eastward drift is a consequence of the viscosity high underneath the Atlantic and the viscosity low underneath the Baltic Shield in the transition zone of the mantle, when compared to the 1D model.

In summary, comparison of the tangential motion of the lateral heterogeneous models shows that the lateral viscosity variations in the transition zone have a strong influence on the tangential motion of model U3L1_V1.

4.6 Conclusions

We have developed a set of 1D and 3D FE flat-earth models with compressible, viscoelastic material properties to study the GIA response induced by an ice-load model simulating the last two cycles of the Late-Pleistocene Fennoscandian ice sheet. The radial dependence of mantle viscosity is based on either results of a formal inverse procedure of the GIA process [Steffen and Kaufmann, 2005], or on an Arrhenius-law. For the 3D models, the lateral viscosity structure has been derived from seismic shear-wave tomography. Model results have been compared to observations of relative sea-level (RSL) changes and crustal velocities (BIFROST data).

We have shown that a consideration of lateral viscosity structure in the Earth's upper mantle significantly influences the crustal velocity predictions, with differences in uplift velocities up to 7 mm/yr. The observed BIFROST crustal velocity data are best fit using a 1D earth model, as for the different 3D earth models deviations between observations and predictions can differ by 2 - 7 mm/yr. The presence of lateral viscosity variations in the upper mantle significantly influences the horizontal velocities, which is the result of a strong horizontal flow component in the 3D earth models. Again, horizontal velocities from the 3D earth model prediction cannot explain the BIFROST data well, the prediction from the 1D earth model scores better. However, we need to stress here that the ice model used has been constructed with a 1D viscoelastic earth model. Thus it is very likely that the better fit of the 1D model prediction is a relict of the ice-model construction. Additionally, our 3D earth models have to be revised, because it is quite unsatisfactory that a less sophisticated 1D model shows better results than a more sophisticated 3D model. For example, chemical variation could be included due to fact that in our models the lateral variations in seismic velocities seen in seismic tomography are caused by lateral temperature variation only. Using another tomography model is also an option. Furthermore, the ice model has to be changed, especially in the central part.

Predictions of RSL curves show significant differences between models with homogeneous and heterogeneous upper mantle of up to more than 150 m. The monotonic land uplift indicated at locations situated within the margins of the former ice sheet is reproduced well by all model predictions. The land subsidence at locations beyond is well modeled (with one exception) by models with homogeneous upper mantle. Models with 3D upper-mantle viscosity structure can only trace the land subsidence at the location of Leeuwarden. Greater differences can be established for the location Lista, where for all models uplift instead of subsidence is predicted. The discrepancies in the values between observations and predictions are possibly a consequence of the coarseness of the FE grid of the ice model. A reason

for the differences especially in the regions beyond the former ice sheet is mainly due to the not perfectly corrected eustatic sea-level change in the sea-level data.

In general, only minor dependencies of the lower-mantle viscosity structure to RSL and crustal motion data can be established, confirming the results of Mitrovica [1996] and Steffen and Kaufmann [2005]. Special investigations to the background model V1 show a strong influence of a laterally varied viscosity in the transition zone to the direction and value of the horizontal velocities. The uplift is mainly influenced by the viscosity structure beneath the lithosphere.

The results demonstrate the complexity of the GIA process and the search for a heterogeneous earth model reproducing observed physical quantities such as surface motions and sea-level data.

Acknowledgments

Many thanks to Kurt Lambeck for providing the FBKS8 ice model. We are grateful for numerous comments and suggestions by two anonymous referees. The figures in this paper are drawn using the GMT graphics package [Wessel and Smith, 1991, 1998]. This research was funded by the DFG (research grant KA1723/1-1).